

# Accurately predicting the escape fraction of ionizing photons using rest-frame ultraviolet absorption lines

J. Chisholm<sup>1</sup>, S. Gazagnes<sup>1,2,3,4</sup>, D. Schaerer<sup>1,5</sup>, A. Verhamme<sup>1</sup>, J. R. Rigby<sup>6</sup>, M. Bayliss<sup>7</sup>, K. Sharon<sup>8</sup>, M. Gladders<sup>9,10</sup>, H. Dahle<sup>11</sup>

<sup>1</sup> Observatoire de Genève, Université de Genève, 51 Ch. des Maillettes, 1290 Versoix, Switzerland

<sup>2</sup> Johan Bernouilli Institute, University of Groningen, P.O. Box 407, 9700 Groningen, AK, The Netherlands

<sup>3</sup> Kapteyn Astronomical Institute, University of Groningen, P.O. Box 800, 9700 AV Groningen, The Netherlands

<sup>4</sup> KVI-Center for Advanced Radiation Technology (KVI-CART), University of Groningen, Zernikelaan 25, Groningen 9747 AA, The Netherlands

<sup>5</sup> CNRS, IRAP, 14 Avenue E. Belin, 31400 Toulouse, France

<sup>6</sup> Observational Cosmology Lab, NASA Goddard Space Flight Center, 8800 Greenbelt Rd., Greenbelt, MD 20771, USA

<sup>7</sup> MIT Kavli Institute for Astrophysics and Space Research, 77 Massachusetts Ave., Cambridge, MA 02139, USA

<sup>8</sup> Department of Astronomy, University of Michigan, 500 Church St., Ann Arbor, MI 48109, USA

<sup>9</sup> Department of Astronomy & Astrophysics, University of Chicago, 5640 S. Ellis Ave., Chicago, IL 60637, USA

<sup>10</sup> Kavli Institute for Cosmological Physics, University of Chicago, 5640 South Ellis Ave., Chicago, IL 60637, USA

<sup>11</sup> Institute of Theoretical Astrophysics, University of Oslo, P.O. Box 1029, Blindern, NO-0315 Oslo, Norway

Received date; accepted date

## ABSTRACT

The fraction of ionizing photons that escape high-redshift galaxies sensitively determines whether galaxies reionized the early universe. However, this escape fraction cannot be measured from high-redshift galaxies because the opacity of the intergalactic medium is large at high redshifts. Without methods to indirectly measure the escape fraction of high-redshift galaxies, it is unlikely that we will know what reionized the universe. Here, we analyze the far-ultraviolet (UV) H I (Lyman series) and low-ionization metal absorption lines of nine low-redshift, confirmed Lyman continuum emitting galaxies. We use the H I covering fractions, column densities, and dust attenuations measured in a companion paper to predict the escape fraction of ionizing photons. We find good agreement between the predicted and observed Lyman continuum escape fractions (within  $1.4\sigma$ ) using both the H I and ISM absorption lines. The ionizing photons escape through holes in the H I, but we show that dust attenuation reduces the fraction of photons that escape galaxies. This means that the average high-redshift galaxy likely emits more ionizing photons than low-redshift galaxies. Two other indirect methods accurately predict the escape fractions: the Ly $\alpha$  escape fraction and the optical [O III]/[O II] flux ratio. We use these indirect methods to predict the escape fraction of a sample of 21 galaxies with rest-frame UV spectra but without Lyman continuum observations. Many of these galaxies have low escape fractions ( $f_{\text{esc}} \leq 1\%$ ), but 11 have escape fractions  $> 1\%$ . The methods presented here will measure the escape fractions of high-redshift galaxies, enabling future telescopes to determine whether star-forming galaxies reionized the early universe.

**Key words.** Cosmology: dark ages, reionization, first stars – Galaxies: irregular – Galaxies: ISM – Galaxies: starburst

## 1. Introduction

In the local universe, gas between galaxies is mostly highly ionized (Fan et al. 2006), but it has not always been that way. Hydrogen recombined at  $z = 1090$  and remained neutral until  $z \sim 7 - 9$  (Planck Collaboration et al. 2016). This is most easily observed by the absorption blueward of rest-frame Ly $\alpha$  (1216Å) in the spectra of  $z > 6$  quasars (the "Gunn-Peterson trough"; Gunn & Peterson 1965; Becker et al. 2001). Some mechanism must have produced copious ionizing photons to reionize the universe.

The source of reionization is one of the core questions that future large observatories, such as the *James Webb* Space Telescope (*JWST*) and extremely large telescopes (ELT), aim to answer. One possibility is that active galactic nuclei (AGN) provided the ionizing photons. However, current observed AGN luminosity functions indicate that there were not enough AGN

to reionize the early universe (Hopkins et al. 2008; Willott et al. 2010; Fontanot et al. 2012; Ricci et al. 2017; Onoue et al. 2017).

An alternative source of ionizing photons is the first generation of high-mass stars. For these stars to matter to reionization, the emissivity of ionizing photons ( $\dot{n}_{\text{ion}}$ ) escaping high-redshift galaxies must exceed the recombination rate. Commonly  $\dot{n}_{\text{ion}}$  is expressed as

$$\dot{n}_{\text{ion}} = f_{\text{esc}} \xi_{\text{ion}} \rho_{\text{UV}}, \quad (1)$$

where  $\xi_{\text{ion}}$  is the intrinsic number of ionizing photons emitted by stars,  $\rho_{\text{UV}}$  is the total ultraviolet (UV) luminosity density, and  $f_{\text{esc}}$  is the absolute fraction of ionizing photons that escape galaxies. More generally, the quantities in Eq. 1 depend on the UV magnitude,  $M_{\text{UV}}$ , and the total  $\dot{n}_{\text{ion}}$  is found by integrating over the UV luminosity function. While highly dependent on clumping and redshift, the estimated  $\Omega_{\text{matter}}$  from  $\Lambda$ CDM indicates that the universe is reionized when

Send offprint requests to: John.Chisholm@unige.ch

$\log(\dot{n}_{\text{ion}}[\text{photons s}^{-1} \text{ Mpc}^{-3}])$  is near 50 – 51 (Madau et al. 1999; Meiksin 2005; Bolton & Haehnelt 2007; Ouchi et al. 2009; Kuhlen & Faucher-Giguère 2012; Robertson et al. 2013, 2015).

In principle, whether or not stars reionized the universe is an observable question. The parameter  $\xi_{\text{ion}}$  is related to the observed H $\alpha$  emission and depends on the metallicity and star formation rate of the galaxies (Leitherer & Heckman 1995; Bruzual & Charlot 2003). Recent studies constrain  $\xi_{\text{ion}}$  at  $z = 6-8$  (Dunlop et al. 2012; Bouwens et al. 2012b; Robertson et al. 2013; Harikane et al. 2017). Similarly, deep *Hubble* Space Telescope (HST) observations have pushed the UV luminosity functions down to fainter  $M_{\text{UV}}$  at high redshifts (Bouwens et al. 2006; Ouchi et al. 2009; Oesch et al. 2014; Finkelstein et al. 2015; Bouwens et al. 2015; Livermore et al. 2017; Oesch et al. 2017). While requiring extraordinary observations, these studies are beginning to constrain  $\xi_{\text{ion}}$  and  $\rho_{\text{UV}}$  during the epoch of reionization.

These observational constraints suggest that  $f_{\text{esc}} \sim 0.1 - 0.2$  if stars reionized the universe (Ouchi et al. 2009; Robertson et al. 2013; Bouwens et al. 2015; Dressler et al. 2015; Robertson et al. 2015; Ishigaki et al. 2017). Whether  $f_{\text{esc}}$  reaches these values has not been observationally confirmed. First, the opacity of the intergalactic medium (IGM) is, on average, too large to observe LyC photons above  $z \sim 4$  (Worseck et al. 2014). Therefore, a direct detection of ionizing photons escaping from a single galaxy during the epoch of reionization is statistically unlikely. Alternatively, studies focused on lower redshift galaxies where the Lyman continuum (LyC;  $< 912\text{\AA}$ ) is directly observable. However, directly detecting ionizing photons at low redshift is still challenging. It requires deep observations of intrinsically faint emission in the very far-UV, which is a notoriously hard regime for high-sensitivity detectors. Only ten individual  $z < 0.4$  galaxies have spectroscopically confirmed  $f_{\text{esc}} > 0$  (Bergvall et al. 2006; Leitert et al. 2011; Borthakur et al. 2014; Izotov et al. 2016a,b; Leitherer et al. 2016; Izotov et al. 2018). Additionally, four such galaxies at  $z \sim 3 - 4$  have been confirmed (Vanzella et al. 2015, 2016; de Barros et al. 2016; Shapley et al. 2016; Bian et al. 2017; Vanzella et al. 2018), after accounting for foreground contamination (e.g., Vanzella et al. 2010). To constrain  $f_{\text{esc}}$  during the epoch of reionization, indirect  $f_{\text{esc}}$  probes available at both high (to measure galaxies in the epoch of reionization) and low redshifts (to confirm the predicted  $f_{\text{esc}}$  values) are required.

We present a new analysis of the rest-frame UV properties of nine confirmed low-redshift galaxies that emit ionizing photons and have publicly available far-UV observations. We use the fits of the stellar continua, interstellar medium (ISM) metal absorption lines, and ISM H I absorption lines (the Lyman series) from Gazagnes et al. (2018) (hereafter Paper I) to constrain the neutral gas and dust attenuation properties. Since the H I and dust are the major sinks of ionizing photons, these measurements allow us to accurately predict  $f_{\text{esc}}$ . These new methods can be used to efficiently select low-redshift galaxies that emit ionizing photons or for future telescopes (such as *JWST* or ELTs) to constrain  $\dot{n}_{\text{ion}}$  of galaxies reionizing the universe.

The structure of this paper is as follows: Sect. 2 introduces the observations of the nine publicly available LyC emitters and summarizes how Paper I fit the Lyman series absorption lines. We use these fits to predict  $f_{\text{esc}}$  (Sect. 3) and explore what fit parameters contribute to the observed  $f_{\text{esc}}$  values (Sect. 4). We then test using the Si II absorption lines (Sect. 5.1), Ly $\alpha$  escape fractions (Sect. 5.2), and the [O III]/[O II] ratios (Sect. 5.3) to indirectly predict  $f_{\text{esc}}$ . In Sect. 6 we apply these indirect methods to galaxies without Lyman series observations to demonstrate

how these methods can be used for high-redshift galaxies. Our main conclusions are summarized in Sect. 7.

## 2. Data and absorption line analysis

### 2.1. Rest-frame far-UV observations

#### 2.1.1. The Lyman continuum emitting sample

In this paper, we predominantly use the rest-frame far-UV spectra of the nine publicly available known LyC emitters (hereafter called the Lyman continuum emitting sample; Borthakur et al. 2014; Izotov et al. 2016a,b; Leitherer et al. 2016) taken with the Cosmic Origins Spectrograph (COS; Green et al. 2012) on the HST. We note that Izotov et al. (2018) recently discovered a tenth Lyman continuum emitter that we do not include in this paper because it is not publicly available (but see Sect. 6.4). As summarized in Chisholm et al. (2017), these nine galaxies have low stellar masses ( $10^8 - 10^{10} M_{\odot}$ ), high star formation rates ( $3 - 77 M_{\odot} \text{ yr}^{-1}$ ), and moderately low gas-phase metallicities ( $12 + \log(\text{O}/\text{H}) = 7.9 - 8.7$ ). Table 1 lists the galaxies in the Lyman continuum emitting sample and their observed Lyman continuum ( $f_{\text{esc}}^{\text{obs}}$ ; Chisholm et al. 2017) and Ly $\alpha$  ( $f_{\text{esc}}^{\text{Ly}\alpha}$ ; Verhamme et al. 2017) escape fractions. Two galaxies, Tol 0440–381 and Mrk 54, have the COS detector gap over the Ly $\alpha$  feature. Therefore, their  $f_{\text{esc}}^{\text{Ly}\alpha}$  values are not measured.

Eight of these nine galaxies were observed with the low-resolution G140L grating (nominal resolution of  $R \sim 1500$ ) on HST/COS, while J0921+4509 was observed with the high-resolution G130M and G160M gratings ( $R \sim 15000$ ). These setups observed the rest-frame Lyman series and Si II 1260 $\text{\AA}$  absorption lines of each galaxy. Each galaxy also has rest-frame optical observations, such that extinction-corrected [O III] 5007 $\text{\AA}$ /[O II] 3727 $\text{\AA}$  flux ratios ( $O_{32}$ ) are measured (last column of Table 1; Verhamme et al. 2017).

The HST/COS G140L data were reduced using the methods outlined in Worseck et al. (2016). Special attention was paid to the pulse heights and extraction apertures of each individual spectrum. The pulse heights and apertures used were outlined in Chisholm et al. (2017). We placed the galaxy into the rest frame using the redshifts from the Sloan Digital Sky Survey (Ahn et al. 2014). We then corrected each spectrum for foreground reddening using the values from Schlegel et al. (1998) and the Milky Way reddening law (Cardelli et al. 1989).

#### 2.1.2. Low-redshift galaxies with unobserved LyC emission

In Sect. 5.3 we extend the Lyman continuum emitting sample to include the full sample from Paper I with measured  $O_{32}$  (see Table 2). This full sample includes four low-redshift galaxies that do not have observations of the Lyman continuum, but have observations of the Lyman series. The full sample includes three Green Pea galaxies (Henry et al. 2015) and one Lyman Break Analog (Heckman et al. 2011, 2015; Alexandroff et al. 2015; Heckman & Borthakur 2016). These four galaxies were also observed with HST/COS and the G130M grating. The data were reduced following the methods outlined in Wakker et al. (2015). These galaxies do not have LyC observations, consequently we predict their LyC escape fractions but we cannot confirm them. In Sect. 5.3 we use the Lyman series observations of the full sample to predict the relation between  $f_{\text{esc}}$  and  $O_{32}$ .

Table 1: Measured properties of the Lyman continuum emitting sample from Gazagnes et al. (2018) in order of decreasing  $f_{\text{esc}}^{\text{obs}}$ .

Galaxy name	$f_{\text{esc}}^{\text{obs}}$	$E_{B-V}$ [mag]	$\log(N_{\text{HI}})$ [ $\log(\text{cm}^{-2})$ ]	$C_f^{\text{H}}$	$C_f^{\text{Si}}$	$f_{\text{esc}}^{\text{pre}}$	$f_{\text{esc}}^{\text{Ly}\alpha}$	$O_{32}$
(1)	(2)	(3)	(4)	(5)	(6)	(7)	(8)	(9)
J115204.9+340050	$0.13 \pm 0.01$	$0.13 \pm 0.02$	$19.43 \pm 0.18$	$0.62 \pm 0.09$	$0.27 \pm 0.14$	$0.08 \pm 0.02$	$0.34 \pm 0.07$	5.4
J144231.4-020952	$0.074 \pm 0.010$	$0.14 \pm 0.02$	$19.69 \pm 0.58$	$0.55 \pm 0.04$	$0.47 \pm 0.19$	$0.09 \pm 0.02$	$0.54 \pm 0.11$	6.7
J092532.4+140313	$0.072 \pm 0.008$	$0.16 \pm 0.02$	$17.81 \pm 3.0^{\text{H}}$	$0.64 \pm 0.09$	$0.41 \pm 0.19$	$0.05 \pm 0.01$	$0.29 \pm 0.06$	4.8
J150342.8+364451	$0.058 \pm 0.006$	$0.27 \pm 0.04$	$19.60 \pm 0.17$	$0.75 \pm 0.06$	$0.45 \pm 0.28$	$0.010 \pm 0.005$	$0.29 \pm 0.06$	4.9
J133304.0+624604	$0.056 \pm 0.015$	$0.15 \pm 0.04$	$19.78 \pm 0.37$	$0.83 \pm 0.07$	$0.39 \pm 0.21$	$0.03 \pm 0.01$	$0.52 \pm 0.11$	4.8
Tol 0440-381	$0.019 \pm 0.010$	$0.27 \pm 0.03$	$19.27 \pm 0.10$	$0.57 \pm 0.08$	$0.37 \pm 0.05$	$0.017 \pm 0.006$	–	2.0
J092159.4+450912	$0.010 \pm 0.001$	$0.22 \pm 0.02$	$18.63 \pm 0.19$	$0.77 \pm 0.12$	$0.60 \pm 0.14$	$0.017 \pm 0.004$	$0.01 \pm 0.01$	0.3
Tol 1247-232	$0.004 \pm 0.002$	$0.16 \pm 0.01$	$19.19 \pm 0.44$	$0.69 \pm 0.08$	$0.26 \pm 0.01$	$0.049 \pm 0.008$	$0.19 \pm 0.01$	3.4
Mrk 54	$< 0.002$	$0.36 \pm 0.01$	$19.37 \pm 0.10$	$0.50 \pm 0.08$	$0.32 \pm 0.01$	$0.007 \pm 0.002$	–	0.4

**Notes.** Column 1 gives the name of the galaxy; column 2 gives the observed escape fraction of ionizing photons ( $f_{\text{esc}}^{\text{obs}}$ ; taken from the recalculations of Chisholm et al. 2017). Column 3 is the stellar continuum attenuation ( $E_{B-V}$ ). Column 4 is the logarithm of the H I column density ( $N_{\text{HI}}$ ) derived from the O I 1039Å absorption line and  $12 + \log(\text{O}/\text{H})$  (except for J0925+1403 where O I is not detected; denoted with an H). Column 5 is the H I covering fraction ( $C_f^{\text{H}}$ ) derived from the depth at line center of the Lyman series absorption lines, and column 6 is the Si II covering fraction ( $C_f^{\text{Si}}$ ). Columns 3–6 are taken from Paper I. Column 7 is the predicted Lyman continuum escape fraction using the dust attenuation and  $C_f^{\text{H}}$  (Eq. 5). Column 8 is the Ly $\alpha$  escape fraction ( $f_{\text{esc}}^{\text{Ly}\alpha}$ ; Verhamme et al. 2017) rescaled to an intrinsic flux ratio of Ly $\alpha$ /H $\alpha$  = 8.7. The extinction-corrected [O III] 5007Å/[O II] 3727Å flux ratio ( $O_{32}$ ) is given in column 9 (Verhamme et al. 2017). We note that Tol 0400-381 and Mrk 54 have the detector gap over the Ly $\alpha$  line, thus they do not have a measured  $f_{\text{esc}}^{\text{Ly}\alpha}$ .

### 2.1.3. High-redshift galaxies from MEGaSAURA

Similarly, in Sect. 6 we focus on 14  $z > 2$  lensed galaxies from The Magellan Evolution of Galaxies Spectroscopic and Ultraviolet Reference Atlas (MEGaSAURA; Rigby et al. 2018). These lensed galaxies have spectra taken with the MagE spectrograph (Marshall et al. 2008) on the Magellan telescopes. The data were reduced using D. Kelson’s pipeline<sup>1</sup> and placed into the observed frame using the redshifts measured from the UV emission lines (Rigby et al. 2018). Two of these galaxies have Lyman series and  $O_{32}$  observations, thus they are included in the full sample (Table 2). The other 12 galaxies do not have Lyman series or  $O_{32}$  observations, and we apply our indirect methods to these spectra in Sect. 6. These high-redshift galaxies do not have measured Lyman continuum escape fractions, but their rest-frame UV spectra test the methods presented in this paper.

### 2.2. Lyman series fitting

To predict the fraction of ionizing photons that escape a galaxy, we determined the H I properties from the Lyman series absorption lines between 920-1025Å. These measurements describe the quantity and porosity of H I along the line of sight. Paper I describes this procedure in detail; here we summarize the process and further details are provided in that paper.

We fit the observed flux density ( $F_{\lambda}^{\text{obs}}$ ) using a linear combination of fully theoretical, STARBURST99 stellar continuum models ( $F_{\lambda}^*$ ; Leitherer et al. 1999). We created these stellar continuum models using the Geneva stellar evolution tracks (Meynet et al. 1994) and the WM-BASIC method (Leitherer et al. 2010), assuming an initial mass function with a high (low) mass exponent of 2.3 (1.3) and a high-mass cutoff at 100  $M_{\odot}$ . These models have a spectral resolution of  $R \sim 2500$ . The final  $F_{\lambda}^*$  is a linear combination of 10 single-age stellar continuum models each with an age between 1 – 40 Myr. The stellar continuum metallicity was chosen as the model closest to the measured gas-phase metallicity. We fit for the linear coefficient multiplied by each

single-aged STARBURST99 model that best matches the data using MPFIT (Markwardt 2009).

We simultaneously reddened  $F_{\lambda}^*$  to account for a uniform foreground dust screen using the attenuation law ( $k_{\lambda}$ ) from Reddy et al. (2016a) and a fitted stellar attenuation value ( $E_{B-V}$ ). In Sect. 3.1 we discuss the implications for the assumed dust geometry.

Finally, we measured the H I and metal ISM absorption line properties by including Lyman series, O VI, O I, C II, C III, and Si II absorption features. We fit for the observed Lyman series absorption lines using the radiative transfer equation, assuming an overlapping covering fraction ( $C_f$ ; Barlow & Sargent 1997; Hamann et al. 1997), which has a functional form of

$$F_{\lambda}^{\text{obs}} = F_{\lambda}^* \times 10^{-0.4E_{B-V}k_{\lambda}} \times (1 - C_f^{\text{H}} + C_f^{\text{H}}e^{-\tau_{\lambda}}), \quad (2)$$

where we fit for  $E_{B-V}$ , the intrinsic stellar continuum ( $F_{\lambda}^*$ ), the optical depth ( $\tau = \sigma N_{\text{HI}}$ ), and the H I covering fraction ( $C_f^{\text{H}}$ ). As discussed in Paper I, the H I lines are saturated ( $\tau_{\lambda} \gg 1$ ), but not damped. Consequently,  $N_{\text{HI}}$  cannot be accurately determined. Therefore, we measured the H I column density from the unsaturated O I 1039Å line, and converted this column density into  $N_{\text{HI}}$  using the observed  $12 + \log(\text{O}/\text{H})$ . One galaxy, J0925+1403, does not have a O I 1039Å detection, therefore we used the fitted  $N_{\text{HI}}$  value and the large associated errors. The fits of Eq. 2 constrain the stellar population, dust and  $N_{\text{HI}}$  properties of the LyC emitters. The Lyman series fits for all of the galaxies are shown in the Appendix of Paper I.

Since the Lyman series is always found to be optically thick (Paper I), we find that  $C_f^{\text{H}}$  is most robustly measured by taking the median of

$$C_f^{\text{H}} = 1 - \frac{F_{\lambda}^{\text{obs}}}{F_{\lambda}^* 10^{-0.4E_{B-V}k_{\lambda}}} \quad (3)$$

in a region that we visually selected near each Lyman series line. To calculate the  $C_f^{\text{H}}$  errors of the individual Lyman series transitions, we varied the observed flux by a Gaussian distribution centered on zero with a standard deviation equal to the flux error. We then measured  $C_f^{\text{H}}$  from this altered flux array and tabulate the result. We repeated the process 1000 times to produce

<sup>1</sup> <http://code.obs.carnegiescience.edu/mage-pipeline>

a distribution of  $C_f^H$  values. We then took the median and standard deviation of this distribution as the  $C_f^H$  estimate and uncertainty. After we measured  $C_f^H$  for each transition, we took the weighted median and standard deviation of all observed Lyman series lines as the  $C_f^H$  estimate and error (see Table 1). We used this method because it does not rely on assumptions about how the  $C_f^H$  changes with velocity, and we could control for the impact of nearby Milky Way absorption lines.

### 2.3. Si II observations

Finally, we measured the Si II covering fraction ( $C_f^{\text{Si}}$ ) in two ways. First, we measured  $C_f^{\text{Si}}$  of the Si II 1260Å line with Eq. 3. This method assumes that the strong Si II 1260Å line, with an oscillator strength of 1.22, is saturated. Second, we calculated  $C_f^{\text{Si}}$  from the Si II 1190Å doublet, which accounts for low Si II optical depths. We took the average and standard deviation of these two values as the  $C_f^{\text{Si}}$  values and errors, respectively. We note that both estimates of  $C_f^{\text{Si}}$  are largely equivalent to each other, implying that the Si II 1260Å line is saturated (see Paper I). Now we have measured the ingredients to predict the Lyman continuum escape fractions.

## 3. Predicting the Lyman continuum escape fraction with the Lyman series

The absolute Lyman continuum escape fraction,  $f_{\text{esc}}$ , is defined as the ratio of the observed ionizing flux to the intrinsic ionizing flux produced by stars,

$$f_{\text{esc}} = \frac{F_{912}^{\text{obs}}}{F_{912}^{\star}}, \quad (4)$$

where  $F_{\lambda}^{\text{obs}}$  is defined in Eq. 2. Since ionizing photons can be absorbed by dust or H I,  $f_{\text{esc}}$  is predicted from the fits to the Lyman series and the dust attenuation as

$$f_{\text{esc}}^{\text{pre}} = 10^{-0.4E_{B-V}k_{912}} \times (1 - C_f^H). \quad (5)$$

The Lyman continuum is optically thick at H I column densities above  $10^{17.7} \text{ cm}^{-2}$ . For column densities below this column density, the gas is optically thin and the escape fraction increases because unabsorbed light escapes. However, in Paper I we used the O I column densities to demonstrate that the  $N_{\text{H}}$  in these galaxies is larger than  $10^{18.63} \text{ cm}^{-2}$ . Therefore, we neglected the last term of Eq. 2 when calculating  $f_{\text{esc}}^{\text{pre}}$ . To calculate  $f_{\text{esc}}^{\text{pre}}$ , we used  $k_{912} = 12.87$  from the attenuation curve of Reddy et al. (2016a). The errors on  $f_{\text{esc}}^{\text{pre}}$  were calculated by propagating the errors of  $E_{B-V}$  and  $C_f^H$  through Eq. 5.

The value  $f_{\text{esc}}^{\text{pre}}$  closely follows  $f_{\text{esc}}^{\text{obs}}$  for the nine galaxies in the Lyman continuum emitting sample (Fig. 1). The normalized absolute difference between  $f_{\text{esc}}^{\text{pre}}$  and  $f_{\text{esc}}^{\text{obs}}$  ( $|f_{\text{esc}}^{\text{obs}} - f_{\text{esc}}^{\text{pre}}|/f_{\text{esc}}^{\text{obs}}$ ) is 48%. The median  $f_{\text{esc}}^{\text{pre}}$  is within  $1.4\sigma$  of  $f_{\text{esc}}^{\text{obs}}$  (i.e., within the 95% confidence interval). This assumes a uniform distribution because the reported  $C_f^H$  and  $E_{B-V}$  errors are highly non-Gaussian. The value  $f_{\text{esc}}^{\text{obs}}$  heavily depends on the modeling of the stellar population. Table 9 of Izotov et al. (2016b) demonstrates that the median  $f_{\text{esc}}^{\text{obs}}$  varies by 0.01 (10-20%) if different stellar population models are used. This error, while not accounted for in the standard  $f_{\text{esc}}^{\text{obs}}$  error bars, would improve the quoted statistics.

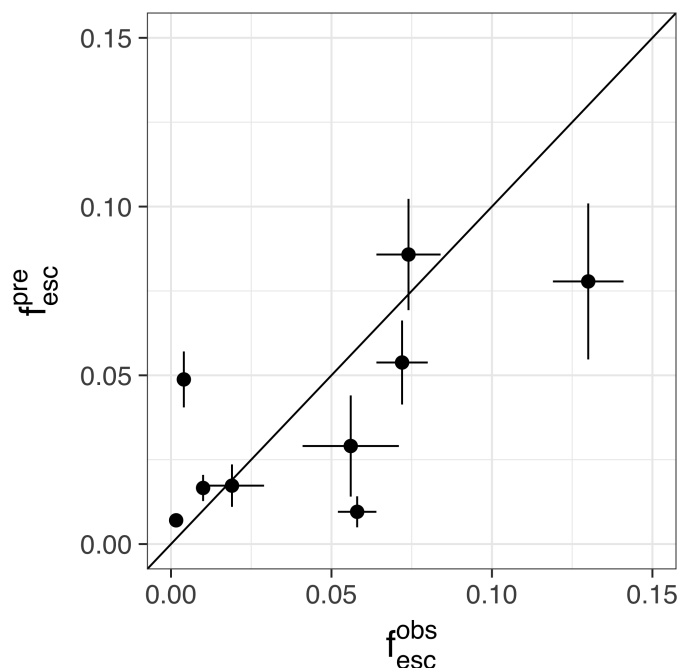


Fig. 1: Plot of the observed Lyman continuum escape fraction ( $f_{\text{esc}}^{\text{obs}}$ ) vs. the predicted Lyman continuum escape fraction ( $f_{\text{esc}}^{\text{pre}}$ ) computed using the observed H I absorption properties and Eq. 5. The solid line shows a one-to-one relation, indicating that the predicted values are within  $1.4\sigma$  of the observed Lyman continuum escape fractions. We note that there are two outliers more than  $3\sigma$  from the one-to-one relation: Tol 1247-232 (at  $f_{\text{esc}}^{\text{pre}} \sim 0.05$  and  $f_{\text{esc}}^{\text{obs}} \sim 0.005$ ) and J1503+3644 (at  $f_{\text{esc}}^{\text{pre}} \sim 0.01$  and  $f_{\text{esc}}^{\text{obs}} \sim 0.06$ ). These outliers are discussed in Sect. 3

Two galaxies have  $f_{\text{esc}}^{\text{pre}}$  more than  $3\sigma$  from  $f_{\text{esc}}^{\text{obs}}$ : Tol 1247-232 and J1503+3644. For Tol 1247-232,  $f_{\text{esc}}^{\text{obs}}$  is challenging to measure because it is a low-redshift galaxy with possible geocoronal Ly $\alpha$  contamination (Chisholm et al. 2017). Other studies, which used the same observations but different reductions and handling of geocoronal Ly $\alpha$ , have measured  $f_{\text{esc}}^{\text{obs}} = 0.045 \pm 0.012$  and  $0.015 \pm 0.005$  (Leitherer et al. 2016; Puschnig et al. 2017, respectively), whereas Chisholm et al. (2017) have measured  $f_{\text{esc}}^{\text{obs}} = 0.004 \pm 0.002$ . These values are more consistent with the derived  $f_{\text{esc}}^{\text{pre}} = 0.049 \pm 0.008$ . In reality, it is remarkable that  $f_{\text{esc}}^{\text{pre}}$  and  $f_{\text{esc}}^{\text{obs}}$  are at all similar. Regardless, we conclude that Eq. 5 accurately reproduces the observed LyC escape fractions to within  $1.4\sigma$ , on average.

### 3.1. Effect of the assumed geometry on $f_{\text{esc}}$

The  $f_{\text{esc}}$  is measured along the line of sight from a star-forming region to the observer and line-of-sight geometric effects could impact  $f_{\text{esc}}$ . To estimate  $f_{\text{esc}}^{\text{pre}}$ , we assumed a uniform dust screen (Eq. 5). This posits that the dust is uniformly distributed along the line of sight to the galaxy. It is worth exploring the effect this assumed geometry has on  $f_{\text{esc}}^{\text{pre}}$ . Detailed discussions on this issue are also provided elsewhere (Zackrisson et al. 2013; Vasei et al. 2016; Reddy et al. 2016b; Gazagnes et al. 2018).

A simple alternative geometry is that the dust only resides within clumpy neutral gas clouds. Between these neutral clouds are dustless and gasless holes, which we call a clumpy geometry.

This geometry alters the radiative transfer equation (Eq. 2) to become

$$F_{\lambda}^{\text{obs, clumpy}} = F_{\lambda}^* \times 10^{-0.4E_{B-V}k_{912}} \times C_f^H e^{-\tau_{\lambda}} + F_{\lambda}^* \times (1 - C_f^H), \quad (6)$$

and the ionizing escape fraction is

$$f_{\text{esc}}^{\text{pre, clumpy}} = C_f^H \times 10^{-0.4E_{B-V}k_{912}} \times e^{-\tau_{\lambda}} + (1 - C_f^H). \quad (7)$$

We note that the clumpy and uniform geometries treat the dust differently. In the clumpy geometry, the dust attenuation acts only on the  $e^{-\tau_{\lambda}}$  term. To remain at the same  $F_{\lambda}^{\text{obs}}$  (or  $f_{\text{esc}}$ ), the  $C_f^H$  and  $E_{B-V}$  of the clumpy geometry must be larger than the uniform geometry. This is because unattenuated light passes through holes in clumpy geometry, forcing the attenuation within the clumps to be stronger, and the holes to be smaller, to match the observed flux.

To test the effect of the geometry, in Paper I we refit  $F_{\lambda}^{\text{obs}}$  from J1152+3400 and J0921+4509, a large and a small  $f_{\text{esc}}^{\text{obs}}$  galaxy, with the clumpy model (Eq. 6). We find that  $C_f^H = 0.912, 0.976$  and  $E_{B-V} = 0.239$  and  $0.236$ , respectively. Both are larger than the uniform dust screen model (Table 1). However, these values and Eq. 7 lead to  $f_{\text{esc}}^{\text{pre}} = 0.088$  and  $0.024$ , statistically consistent with  $f_{\text{esc}}^{\text{pre}}$  using the uniform screen (0.08 and 0.016 respectively).

The fitted values ( $E_{B-V}$ ,  $C_f^H$ ) change to match  $F_{\lambda}^{\text{obs}}$  based on the assumed geometry. Therefore, parameters such as  $C_f^H$  and  $E_{B-V}$  are model dependent. However,  $f_{\text{esc}}$  is model independent because the best combination of the model and the parameters are fit to match the data (as discussed in Paper I). The geometry must be accounted for — and remembered — when comparing and interpreting  $C_f$  and  $E_{B-V}$ , but the  $f_{\text{esc}}$  values do not strongly depend on the assumed geometry.

#### 4. Parameters contributing to the predicted escape fractions

The previous section showed that the fits to the observed flux accurately predict the escape fraction of ionizing photons. H I column density, H I covering fraction, and dust attenuation determine these fits. The natural question is which parameters contribute to the predicted escape fractions? In the next three subsections we explore the contribution of each estimated parameter to the predicted escape fractions. We note that the following analysis does not refit the data to maximize the contribution of each parameter, rather it uses the previous fits to answer which parameters contribute to the predicted escape fractions.

##### 4.1. H I column density

The first parameter that we discuss is  $N_{\text{HI}}$ . If  $N_{\text{HI}}$  is low enough, ionizing photons pass through the ISM unabsorbed (a "density-bounded" region; Jaskot & Oey 2013; Zackrisson et al. 2013; Nakajima & Ouchi 2014). The escape fraction of ionizing photons only due to  $N_{\text{HI}}$  is

$$f_{\text{esc}}^{\text{NH}} = e^{-\sigma N_{\text{HI}}}, \quad (8)$$

where  $\sigma$  is the photoionization cross section ( $6.3 \times 10^{-18} \text{ cm}^2$ ). We set  $C_f^H = 1$  and  $E_{B-V} = 0$  in Eq. 5. The  $f_{\text{esc}}^{\text{NH}}$  values are too low to match  $f_{\text{esc}}^{\text{obs}}$  (red circles in Fig. 2). This implies that the H I along the line of sight is optically thick (see the discussion in Paper I).

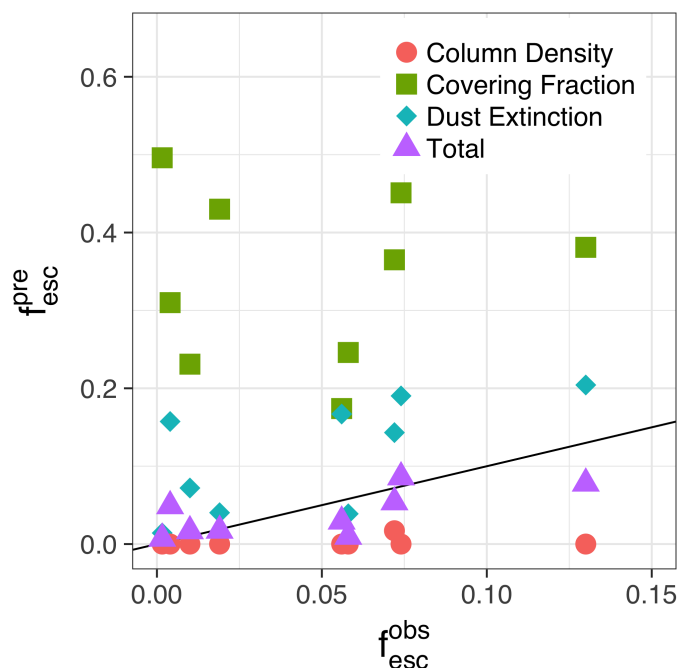


Fig. 2: Observed Lyman continuum escape fraction ( $f_{\text{esc}}^{\text{obs}}$ ) vs. the Lyman continuum escape fractions predicted by isolating various fit parameters ( $f_{\text{esc}}^{\text{pre}}$ ). Each colored symbol represents the contribution of a single parameter from our model (Eq 5). The red circles correspond to the contribution to the escape fraction from the H I column density alone. The cyan diamonds correspond to the contribution from dust attenuation only. The green squares indicate the contribution to  $f_{\text{esc}}^{\text{pre}}$  from the H I covering fraction. The purple triangles show the combination of all three mechanisms that scatter about the one-to-one line. Dust and the H I covering fraction dominate  $f_{\text{esc}}^{\text{pre}}$ .

##### 4.2. Covering fraction

The second parameter, the covering fraction, implies that ionizing photons escape through holes in the H I gas (Heckman et al. 2011). If we assumed no attenuation from dust ( $E_{B-V} = 0$ ) and that H I is optically thick, the predicted escape fractions are

$$f_{\text{esc}}^{\text{CF}} = 1 - C_f^H, \quad (9)$$

which is greater than 0 for the nine Lyman continuum emitters (green squares in Fig. 2). However, these  $f_{\text{esc}}^{\text{CF}}$  values are substantially higher than  $f_{\text{esc}}^{\text{obs}}$ . If holes in the H I were solely responsible for the escape of ionizing photons, and there was no dust, the escape fractions would be much higher than observed.

Several previous studies have used  $f_{\text{esc}}^{\text{CF}}$  to estimate  $f_{\text{esc}}$ , but overestimated the  $f_{\text{esc}}$  values (Quider et al. 2009; Heckman et al. 2011; Jones et al. 2012, 2013; Leethochawalit et al. 2016; Vasei et al. 2016). For example, Quider et al. (2009) obtained  $f_{\text{esc}}^{\text{CF}} \sim 0.4$  for the Cosmic Horseshoe, but this disagrees with the upper limit of the absolute  $f_{\text{esc}} < 0.02$  derived with HST imaging by Vasei et al. (2016). However, Quider et al. (2009) did not account for dust attenuation when deriving  $f_{\text{esc}}$ . In Sect. 6.1 we show that accounting for dust leads to  $f_{\text{esc}}$  values that are consistent with the HST observations of the Cosmic Horseshoe.

### 4.3. Dust attenuation

The final contributor to the escape of ionizing photons in our fits is dust. Dust heavily impacts the observed stellar continuum at 912Å: even small  $E_{B-V}$  values lead to large attenuations. J1152+3400, with the smallest  $E_{B-V}$  in the Lyman continuum emitting sample, has an  $A_{912} = 1.7$  mag ( $\tau_{912} = 1.5$ ). Consequently, even small dust attenuation removes significant amounts of ionizing photons.

The effect of dust is maximized in the idealistic case where there is only dust and no H I along the line of sight ( $C_f^H = 1$  and  $\tau = 0$ ). In this case, dust regulates the escape of ionizing photons. The contribution to the escape fraction solely from dust ( $f_{\text{esc}}^D$ ) is calculated as

$$f_{\text{esc}}^D = 10^{-0.4E_{B-V}k_{912}}, \quad (10)$$

where  $f_{\text{esc}}^D$  values are the closest to  $f_{\text{esc}}^{\text{obs}}$  of the three parameters (cyan diamonds in Fig. 4). Nonetheless,  $f_{\text{esc}}^D$  is still too high to match  $f_{\text{esc}}^{\text{obs}}$ , and the combination of dust and  $C_f^H$  are required to match the modeled  $f_{\text{esc}}^{\text{pre}}$  (see purple triangles in Fig. 2).

The individual values of  $E_{B-V}$  and  $C_f^H$  change depending on the assumed geometry (Sect. 3.1; Paper I). However, this does not diminish the contribution of either dust or  $C_f^H$  to  $f_{\text{esc}}^{\text{pre}}$ . In an alternative geometry, the clumpy geometry (Eq. 6), the observed flux far from optically thick H I lines (at wavelengths where  $\tau_\lambda$  is small) is heavily influenced by the product of  $10^{-0.4E_{B-V}k_\lambda}C_f^H$ . Since most of the fitted wavelengths are actually in the small  $\tau_\lambda$  regime, the attenuation significantly influences the fitted  $C_f^H$  value. While the exact contribution of dust and covering fraction are model dependent,  $f_{\text{esc}}^{\text{pre}}$  depends on both.

### 4.4. Connecting low attenuation to high-redshift leakers

We find that dust attenuation strongly contributes to the predicted escape fractions. Consequently, low-mass–or equivalently low-metallicity–galaxies are ideal targets to emit ionizing photons. These properties are similar to the host galaxy properties of known local emitters (Izotov et al. 2016b; Chisholm et al. 2017). Galaxies in the early universe should naturally have these properties (Bouwens et al. 2012a; Madau & Dickinson 2014) and may have higher  $f_{\text{esc}}$  than local galaxies. Schaerer & de Barros (2010) found that typical  $< 10^{10} M_\odot$  galaxies at  $z = 6 - 8$  have  $A_V < 1$ . This implies that  $f_{\text{esc}} > 0.05(1 - C_f^H)$  for galaxies expected to reionize the universe. Using the median  $C_f^H$  from the Lyman continuum emitting sample ( $C_f^H = 0.64$ ),  $z = 6 - 8$  galaxies should have  $f_{\text{esc}} > 0.02$ , much higher than the average galaxy at  $z = 0$ . Further, all of the  $z \sim 3 - 4$  confirmed LyC emitters have  $E_{B-V} < 0.11$  mag, or  $f_{\text{esc}} > 0.27(1 - C_f^H)$  (de Barros et al. 2016; Shapley et al. 2016; Bian et al. 2017). Using the median  $C_f^H$  from our Lyman continuum emitting sample, this corresponds to  $f_{\text{esc}} > 0.1$ , which agrees with the  $f_{\text{esc}}$  required to reionize the universe at  $z = 6 - 8$ . Galaxies in the epoch of reionization likely have low dust attenuations, which makes them ideal candidates to emit a high fraction of their ionizing photons.

## 5. Indirectly predicting the Lyman continuum escape fraction

Directly measuring  $f_{\text{esc}}^{\text{obs}}$  requires deep rest-frame far-UV observations. This means that only a dozen galaxies are confirmed LyC emitters at any redshift. While the Lyman series accurately

predicts the escape fraction (Fig. 1), the Lyman series is also not observable at high redshifts because the opacity of the circumgalactic medium is large. Therefore, we explored ancillary, indirect methods that can predict the  $f_{\text{esc}}$  of high-redshift galaxies. First we explored using the Si II covering fraction to predict the escape fraction. Then we used the observed Ly $\alpha$  escape fraction to approximate  $f_{\text{esc}}$ . Finally, we used the ratio of the optical oxygen emission lines ( $O_{32}=[O\text{ III}] 5007\text{\AA}/[O\text{ II}] 3727\text{\AA}$ ). In Sect. 6, we illustrate how these three methods predict  $f_{\text{esc}}^{\text{pre}}$  for galaxies that are not in our full sample because they do not have publicly available Lyman series observations.

### 5.1. Using Si II absorption

Si II has multiple absorption lines in the rest-frame far-UV, including the 1190 Å doublet and 1260 Å singlet. The ionization potential of Si II (16 eV) means that it probes partially neutral gas, and many studies have used it to diagnose LyC emitters (Heckman et al. 2011; Jones et al. 2012, 2013; Alexandroff et al. 2015; Chisholm et al. 2017). In Paper I, we showed that  $C_f^H$  and the Si II covering fraction ( $C_f^{\text{Si}}$ ) are linearly related, but not equal. We fit the relationship between  $C_f^H$  and  $C_f^{\text{Si}}$  as

$$C_f^{\text{pre, H}} = (0.6 \pm 0.1) \times C_f^{\text{Si}} + (0.5 \pm 0.1). \quad (11)$$

This relationship is significant at the  $3\sigma$  significance level (p-value  $< 0.001$ ). This relation is statistically consistent with the relationship between Si II 1260Å and H I found for  $z \sim 3$  galaxies in Reddy et al. (2016b). In Paper I, we posited that this relation arises because metals do not completely trace the same gas as H I, and  $C_f^{\text{Si}}$  must be corrected to account for this differential covering. A multiple linear regression demonstrates that the constant in Eq. 11 (0.6) depends on the gas-phase metallicity of the galaxy. This indicates that at lower metallicities the Si II traces a lower fraction of the H I.

We predicted the escape fraction of ionizing photons using the Si II absorption lines as

$$f_{\text{esc}}^{\text{pre, Si}} = 10^{-0.4E_{B-V}k_{912}}(1 - C_f^{\text{pre, H}}), \quad (12)$$

where we used  $k_{912} = 12.87$ , the observed  $E_{B-V}$ , and  $C_f^{\text{pre, H}}$  from Eq. 11. The value  $f_{\text{esc}}^{\text{pre, Si}}$  is consistent with  $f_{\text{esc}}^{\text{obs}}$  for the nine known Lyman continuum emitters (left panel of Fig. 3). The difference between  $f_{\text{esc}}^{\text{pre, Si}}$  and  $f_{\text{esc}}^{\text{obs}}$  is 46% of the measured  $f_{\text{esc}}^{\text{obs}}$  values. Similarly, the median  $f_{\text{esc}}^{\text{pre, Si}}$  is within  $1.2\sigma$  of  $f_{\text{esc}}^{\text{obs}}$ . Using the Si II absorption predicts the observed escape fractions with similar accuracy as the Lyman series.

### 5.2. Using Ly $\alpha$ escape fractions

Ionizing photons and Ly $\alpha$  photons are related because H I gas absorbs or scatters both (Verhamme et al. 2015). The Ly $\alpha$  escape fraction is calculated as

$$f_{\text{esc}}^{\text{Ly}\alpha} = \frac{(F[\text{Ly}\alpha]/F[\text{H}\alpha])_{\text{obs}}}{(F[\text{Ly}\alpha]/F[\text{H}\alpha])_{\text{int}}}, \quad (13)$$

where  $(F[\text{Ly}\alpha]/F[\text{H}\alpha])_{\text{obs}}$  is the observed ratio of the Ly $\alpha$  flux to the extinction-corrected H $\alpha$  flux, and  $(F[\text{Ly}\alpha]/F[\text{H}\alpha])_{\text{int}}$  is the theoretical intrinsic flux ratio (which has a value of 8.7 for Case B recombination and a temperature of  $10^4$  K). The  $f_{\text{esc}}^{\text{Ly}\alpha}$  measures the fraction of Ly $\alpha$  photons that escape and

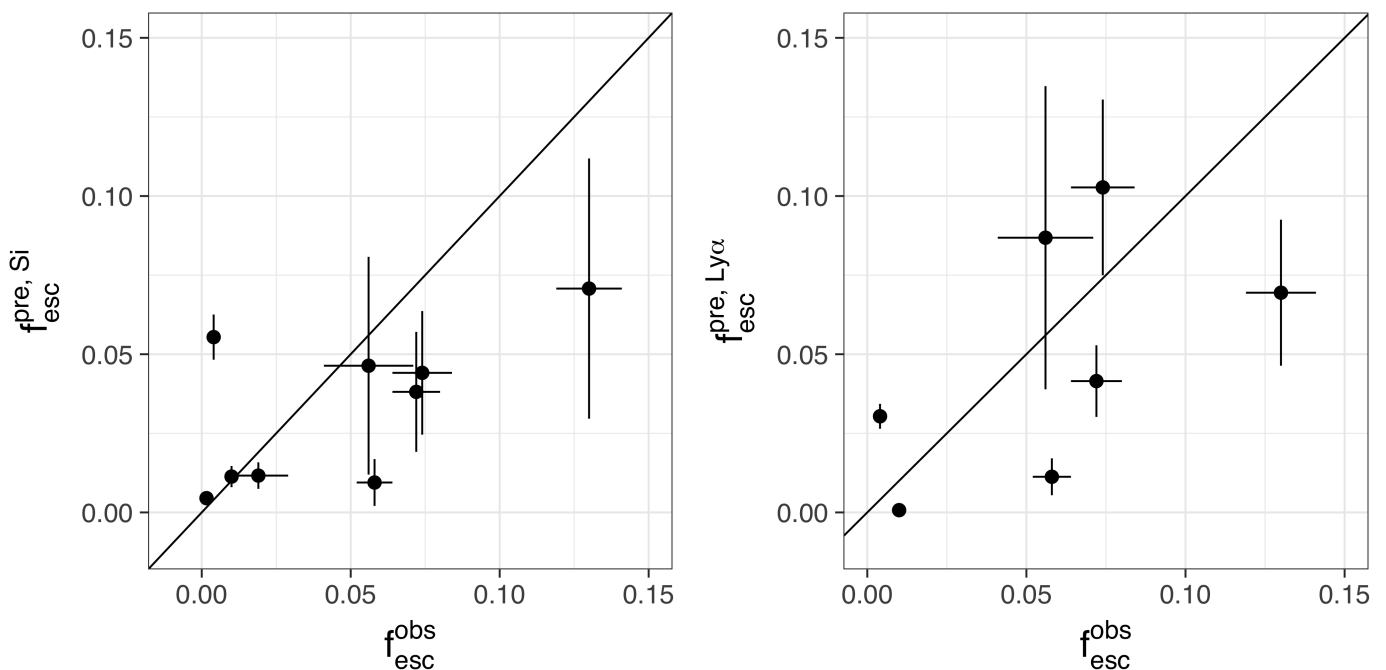


Fig. 3: *Left panel:* Plot of the observed Lyman continuum escape fraction ( $f_{\text{esc}}^{\text{obs}}$ ) vs. the predicted Lyman continuum escape fractions made using the Si II covering fraction, derived from the Si II 1260Å and Si II 1190Å doublet. *Right panel:* The escape fraction predicted by extinction correcting the Ly $\alpha$  escape fraction ( $f_{\text{esc}}^{\text{pre, Ly}\alpha}$ ). The  $f_{\text{esc}}^{\text{pre, Si}}$  and  $f_{\text{esc}}^{\text{pre, Ly}\alpha}$  methods are consistent with the  $f_{\text{esc}}^{\text{obs}}$  within 1.2 and 1.8 $\sigma$ , respectively. There are two fewer  $f_{\text{esc}}^{\text{pre, Ly}\alpha}$  points because Ly $\alpha$  is in the detector gap for Tol 0440–381 and Mrk 54.

does not directly depend on how the Ly $\alpha$  photons escapes. Consequently, we assumed that the only difference between  $f_{\text{esc}}$  and  $f_{\text{esc}}^{\text{Ly}\alpha}$  is the dust attenuation, and used the Ly $\alpha$  escape fraction to predict the LyC escape fraction ( $f_{\text{esc}}^{\text{pre, Ly}\alpha}$ ) as

$$f_{\text{esc}}^{\text{pre, Ly}\alpha} = 10^{-0.4E_{\text{B-V}}k_{912}} f_{\text{esc}}^{\text{Ly}\alpha}. \quad (14)$$

This implies that the LyC and Ly $\alpha$  escape fractions are similar, but that the LyC escape fraction is lower because the dust attenuation is larger at 912Å than at 1216Å. Consequently, Eq. 14 effectively extinction corrects the Ly $\alpha$  escape fraction to predict  $f_{\text{esc}}$ . These values are consistent with  $f_{\text{esc}}^{\text{obs}}$  for the seven galaxies with measured  $f_{\text{esc}}^{\text{Ly}\alpha}$  (right panel of Fig. 3). The average relative difference between  $f_{\text{esc}}^{\text{obs}}$  and  $f_{\text{esc}}^{\text{pre, Ly}\alpha}$  is 55% of  $f_{\text{esc}}^{\text{obs}}$ , and  $f_{\text{esc}}^{\text{pre, Ly}\alpha}$  is, on average, within 1.8 $\sigma$  of  $f_{\text{esc}}^{\text{obs}}$ . The consistency of  $f_{\text{esc}}^{\text{pre, Ly}\alpha}$  is comparable to the two previous  $f_{\text{esc}}^{\text{pre}}$  measurements.

The similar  $f_{\text{esc}}^{\text{pre}}$  and  $f_{\text{esc}}^{\text{pre, Ly}\alpha}$  values are driven by the similar attenuations because the attenuation dominates  $f_{\text{esc}}^{\text{pre}}$  (Sect. 4). The difference in calculating  $f_{\text{esc}}^{\text{pre, Ly}\alpha}$  and  $f_{\text{esc}}^{\text{pre}}$  are the  $C_f^{\text{H}}$  and  $f_{\text{esc}}^{\text{Ly}\alpha}$  values (compare Eq. 5 and Eq. 14). This implies that  $f_{\text{esc}}^{\text{Ly}\alpha}$  and  $C_f^{\text{H}}$  are causally related (Dijkstra et al. 2016; Verhamme et al. 2017).

### 5.3. Using $O_{32}$

Historically, it was challenging to find galaxies emitting ionizing photons. A breakthrough came by selecting samples based on the [O III] 5007Å/[O II] 3727Å flux ratio ( $O_{32}$ ), compactness, and large H $\beta$  equivalent widths. Izotov et al. (2016a), Izotov et al. (2016b), and Izotov et al. (2018) found six out of six galaxies with  $O_{32} > 4$  had  $f_{\text{esc}}^{\text{obs}} > 0.05$ . This selection technique appears

to efficiently select galaxies that emit ionizing photons based on their easily observed rest-frame optical properties. If this selection criteria is universally applicable, it is a powerful technique to select LyC emitting galaxies. It enabled Faisst (2016) to extend local  $O_{32}$  scaling relations to high redshifts to predict that  $z > 6.5$  galaxies could reionize the universe.

To test the effect of  $O_{32}$  on the ionizing escape fraction, we used the full sample of 15 galaxies with predicted  $f_{\text{esc}}^{\text{pre}}$  using the Lyman series (Eq. 5) and  $O_{32}$  measurements from Paper I; the Cosmic Eye and J1429+0643 are excluded because they do not have measured  $O_{32}$ , and GP 0303–0759 is excluded due to Milky Way contamination. By including these six galaxies, with unobserved LyC emission, we extended the  $O_{32}$  dynamic range and derived a relationship between  $O_{32}$  and  $f_{\text{esc}}^{\text{pre}}$  (Fig. 4).

We first explored whether  $O_{32}$  scales with  $f_{\text{esc}}^{\text{pre}}$ . We tested a variety of models for the scaling of the two variables: linearly, quadratically, or as a logarithm of each (or both) variable. We maximized the F-statistic for a model where the variables scale as  $f_{\text{esc}}^{\text{pre}} - O_{32}^2$ . This relationship is significant at the 3 $\sigma$  significance (p-value < 0.001;  $R^2 = 0.61$ ; Fig. 4). A linear regression (see the line in Fig. 4, with the shaded 95% confidence region) gives a relationship of

$$f_{\text{esc}}^{\text{pre, O}} = (0.0017 \pm 0.0004) O_{32}^2 + (0.005 \pm 0.007). \quad (15)$$

This predicts  $f_{\text{esc}}$  using easily observed rest-frame optical emission lines.

Fig. 4 also shows the empirical relationship from Faisst (2016). The two relations are discrepant at  $O_{32}$  values corresponding to  $f_{\text{esc}} > 0.05$ . Eq. 15 predicts that more than 10% of the ionizing photons escape galaxies when  $O_{32} > 5.7$ . Using the extrapolation of  $O_{32}$  with redshift from Faisst (2016), the average galaxy does not have  $f_{\text{esc}} = 0.1$  until  $z \sim 11$ .

Table 2: Measured properties for the 7 galaxies from Gazagnes et al. (2018) without observed Lyman continuum escape fractions.

Galaxy Name	$z$	$E_{B-V}$ [mag]	$C_f^H$	$f_{\text{esc}}^{\text{pre}}$ [ $\times 10^{-3}$ ]	$O_{32}$
(1)	(2)	(3)	(4)	(5)	(6)
J092600.4+442736 <sup>a</sup>	0.18069	$0.11 \pm 0.01$	$0.81 \pm 0.05$	$50 \pm 10$	3.2
GP 1244+0216 <sup>b</sup>	0.23942	$0.29 \pm 0.04$	$0.95 \pm 0.13$	$2 \pm 1$	3.2
GP 1054+5238 <sup>b</sup>	0.25264	$0.20 \pm 0.04$	$0.89 \pm 0.16$	$10 \pm 4$	2.5
GP 0911+1831 <sup>b</sup>	0.26223	$0.35 \pm 0.04$	$0.77 \pm 0.12$	$4 \pm 2$	1.8
SGAS J152745.1+065219 <sup>c</sup>	2.7628	$0.37 \pm 0.002$	$0.99 \pm 0.04$	$0.1 \pm 0.010$	1.6
SGAS J122651.3+215220 <sup>c</sup>	2.9260	$0.20 \pm 0.001$	$1.00 \pm 0.01$	$0.35 \pm 0.01$	1.4
GP 0303–0759 <sup>b</sup>	0.16488	$0.12 \pm 0.05$	–	–	7.3
J142947.00+064334.9 <sup>a</sup>	0.1736	$0.11 \pm 0.02$	$0.96 \pm 0.06$	$10 \pm 1$	–
The Cosmic Eye <sup>c</sup>	3.0748	$0.41 \pm 0.01$	$1.00 \pm 0.02$	$0.016 \pm 0.0005$	–

**Notes.** Column 1 gives the galaxy name listed in descending  $O_{32}$  order. Column 2 gives the redshifts of the galaxies. Column 3 is the stellar attenuation ( $E_{B-V}$ ) measured using the stellar continuum fitting of Paper I. Column 4 is the H I covering fraction measured from the depths of the Lyman series lines ( $C_f^H$ ). Column 5 is the predicted Lyman continuum escape ( $f_{\text{esc}}^{\text{pre}}$ ) calculated using the Lyman series absorption properties. The sixth column gives the [O III] 5007Å/[O II] 3727Å flux ratio ( $O_{32}$ ). We note that GP 0303–0759, J142947.00+064334.9, and the Cosmic Eye (the three galaxies below the horizontal line) are not included in Sect. 5.3 because GP 0303–0759 does not have a measured  $C_f^H$  owing to a Milky Way absorption line, and J142947.00+064334.9 and the Cosmic Eye do not have literature  $O_{32}$  values.

**References.** (a) Heckman et al. (2011, 2015); Alexandroff et al. (2015); Heckman & Borthakur (2016) (b) Henry et al. (2015) (c) Wuyts et al. (2012); Rigby et al. (2018)

$z \sim 11$  is marginally consistent with the  $z_{\text{re}} = 8.8_{-1.4}^{+1.7}$  redshift of instantaneous reionization derived from the combination of the Planck lensing and polarization studies (Planck Collaboration et al. 2016).

Fig 4 also compares Eq. 15 to a similar trend found by Izotov et al. (2018). These authors used a recently discovered galaxy, J1154+2443 with an exceptionally high  $f_{\text{esc}}^{\text{obs}} = 0.46$  to derive a relationship between  $O_{32}$  and  $f_{\text{esc}}^{\text{obs}}$  (the dot-dashed green curve in Fig. 4). Many of our  $f_{\text{esc}}^{\text{pre}}$  values agree with the Izotov et al. (2018) relation and the two relationships are consistent for  $f_{\text{esc}}^{\text{pre}}$  values up to  $f_{\text{esc}} \sim 0.1$ . However, the Izotov et al. (2018) relationship increases more rapidly at higher  $O_{32}$  and  $f_{\text{esc}}^{\text{pre}}$  values than Eq. 15 does. This is apparent from the galaxy J1154+2443, which has  $O_{32} = 11.5 \pm 1$ . The expected  $f_{\text{esc}}^{\text{pre}, O}$ ,  $0.26 \pm 0.06$ , is nearly  $3\sigma$  lower than  $f_{\text{esc}}^{\text{obs}}$ . This suggests that Eq. 15 may steepen at larger  $O_{32}$ , but the steep portion of the Izotov et al. (2018) trend is largely driven by the one high  $f_{\text{esc}}^{\text{obs}}$  galaxy. If Eq. 15 steepens at higher  $O_{32}$  then the redshift required for galaxies to emit 10% of their ionizing photons would be lower than  $z \sim 11$ . Further observations, probing a uniform and large range of  $O_{32}$ , are required to refine Eq. 15.

Studies often use low  $N_{\text{HI}}$  values to explain the correlation between  $f_{\text{esc}}$  and  $O_{32}$  (so-called "density-bounded" regimes; Jaskot & Oey 2013; Zackrisson et al. 2013; Nakajima et al. 2013). However,  $O_{32}$  arises both from high ionization parameter (as required in the density-bounded regime) and from low metallicities (Nagao et al. 2006; Nakajima & Ouchi 2014; Shapley et al. 2015; Sanders et al. 2016; Chisholm et al. 2017; Strom et al. 2017). As shown in Paper I and Fig. 2, LyC photons escape because the H I covering fraction and dust attenuation are low, not because the H I column density is low. Rather, the low attenuation likely connects  $O_{32}$  and  $f_{\text{esc}}$ . Low attenuation could be related to high ionization parameters (dust is destroyed) and/or low metallicities (dust is not created). In this scenario, the lower dust content could mean that there are not enough metals to uniformly fill the gas, or that there are not enough metals to efficiently cool the gas. Both result in channels with little dust or H I along the line of sight, allowing for more ionizing photons to

escape the galaxy. We find a  $2\sigma$  trend between  $O_{32}$  and  $E_{B-V}$  in our sample. Thus, the correlation between  $f_{\text{esc}}$  and  $O_{32}$  may reflect the low dust attenuation of LyC emitters. However, further observations, spanning a large range of  $O_{32}$ , and more theoretical work are required to confirm and understand this observed correlation.

#### 5.4. Using multiple methods to predict $f_{\text{esc}}$

Above, we demonstrated that the Si II absorption lines,  $f_{\text{esc}}^{\text{Ly}\alpha}$ , and  $O_{32}$  consistently predict  $f_{\text{esc}}^{\text{obs}}$ , but the  $O_{32}$  method needs further data to verify. These three prediction methods have similar deviations from  $f_{\text{esc}}^{\text{obs}}$  as using the H I absorption lines. However, the individual methods do not always precisely reproduce  $f_{\text{esc}}^{\text{obs}}$ . If the LyC cannot be directly observed, then  $f_{\text{esc}}^{\text{pre}}$  should be calculated using as many of the three methods as possible. The mean and standard deviation of the three different methods then approximates  $f_{\text{esc}}^{\text{pre}}$ . As an example, Tol 1247–232 has a largely discrepant  $f_{\text{esc}}^{\text{pre}}$ , but when the average of  $f_{\text{esc}}^{\text{pre}, \text{Ly}\alpha}$ ,  $f_{\text{esc}}^{\text{pre}, \text{Si}}$ , and  $f_{\text{esc}}^{\text{pre}, O}$  are taken  $f_{\text{esc}}^{\text{pre}} = 0.038 \pm 0.022$ , which is consistent, within  $2\sigma$ , with  $f_{\text{esc}}^{\text{obs}}$ . Estimating  $f_{\text{esc}}$  with multiple methods reduces the systematic errors of individual observations and produces more consistent  $f_{\text{esc}}$  predictions. We illustrate this in the next section with observations of both high- and low-redshift galaxies.

It is important to produce a statistical sample of predicted  $f_{\text{esc}}$  values with all of the different methods to determine the systematics of each method. For instance, direct observations of the LyC, as well as  $f_{\text{esc}}$  inferred from the Lyman series, Ly $\alpha$ , and Si II lines are all line-of-sight geometry dependent estimates of  $f_{\text{esc}}$ , such that the inferred value substantially changes whether the orientation is through a hole in the H I or through an H I cloud. Conversely, the  $O_{32}$  ratio depends less on the geometry because the ISM is relatively optically thin to the [O III] and [O II] emission. These effects may be imprinted on the different predicted  $f_{\text{esc}}$  values, and variations in  $f_{\text{esc}}^{\text{pre}}$  may illustrate physical geometric variations in LyC emitting galaxies.



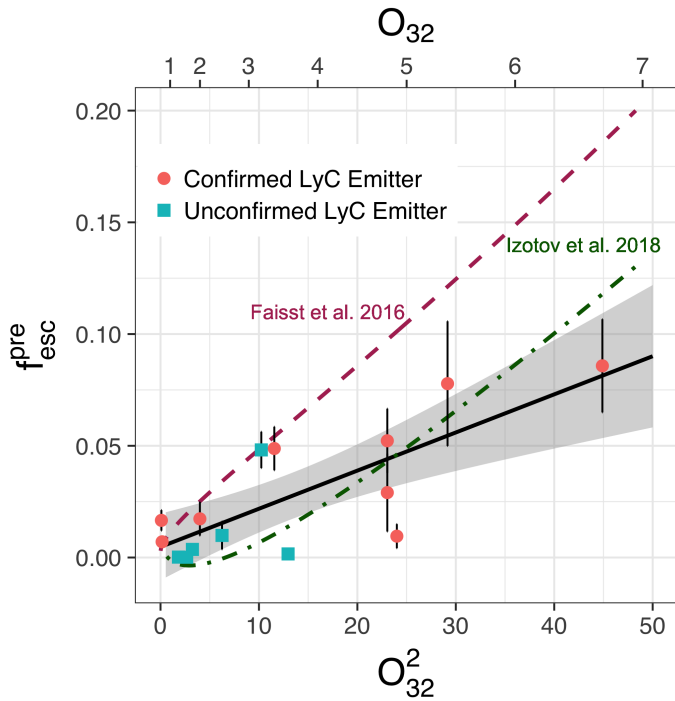


Fig. 4: Plot of the predicted Lyman continuum escape fraction ( $f_{\text{esc}}^{\text{pre}}$ ) from the Lyman series fits (Eq. 5) vs.  $O_{32}$  ( $O_{32} = [\text{O III } 5007\text{\AA}] / [\text{O II } 3727\text{\AA}]$ ) for the full sample from Paper I. The upper x-axis shows the corresponding linear  $O_{32}$  values. Red circles and blue squares denote confirmed and unconfirmed (i.e., galaxies without LyC observations) LyC emitters, respectively. The correlation (Eq. 15) has a  $3\sigma$  significance ( $p$ -value  $< 0.001$ ) and the 95% confidence interval is shown in gray. Overplotted as a maroon dashed line is the empirical relationship from Faisst (2016). The recent fit from Izotov et al. (2018) is also shown as the green dot-dashed line. The relationship derived here predicts lower  $f_{\text{esc}}$  values at large  $O_{32}$  than the two other relationships.

## 6. Predicting the Lyman continuum escape fraction of galaxies without Lyman series observations

The relations presented in the previous section enable estimation of  $f_{\text{esc}}$ , even if the Lyman continuum or Lyman series are not observable. This is especially important for  $z > 4$  galaxies because the IGM transmission of the LyC is  $< 38\%$  at  $z > 4$  (Songaila 2004), making LyC detections even more challenging. The three indirect probes in the previous section may be the only way to estimate the emissivity of high-redshift galaxies reionizing the universe (Eq. 1). We test the methods of Sect. 5 by fitting the rest-frame UV spectra between 1200 – 1500Å of a few test cases in the same manner as we did in Sect. 5. These test cases are the Cosmic Horseshoe, the MEGaSaURA sample, Haro 11, a recently discovered strong LyC emitter from Izotov et al. (2018), and high-redshift confirmed LyC emitters. Because of the uncertainty of the  $O_{32}$  relation (see Sect. 5.3), we only comment on what the observed  $O_{32}$  values imply for  $f_{\text{esc}}^{\text{pre}}$ . Table 3 lists the parameters used to predict the escape fractions for each galaxy.

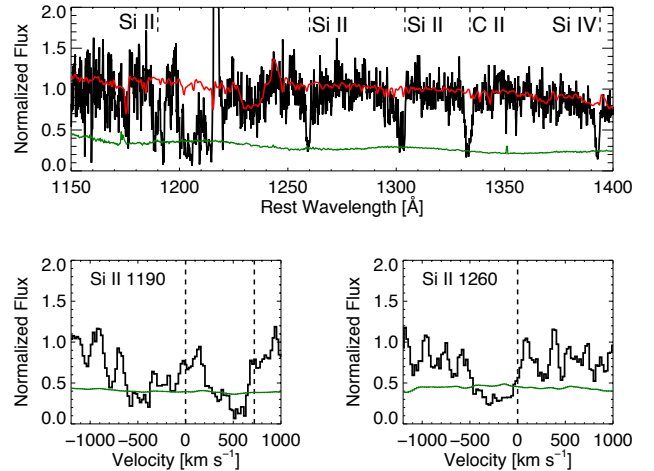


Fig. 5: *Top panel:* Rest-frame UV spectra between 1150 – 1400Å of the Cosmic Horseshoe, a  $z = 2.38$  gravitationally lensed galaxy from the MEGaSaURA sample (Rigby et al. 2018). Overplotted in red is the best-fit STARBURST99 stellar continuum fit. This fit measures  $E_{B-V} = 0.16$  mag. The error spectrum is included underneath in dark green. *Bottom panels:* The Si II 1190Å doublet (left) and Si II 1260Å singlet (right). The corresponding  $C_f^{\text{Si}}$  from the Si II 1260Å line is 0.77. Vertical dashed lines indicate the zero velocity of the various strong ISM metal absorption lines (labeled in the upper panel).

### 6.1. The Cosmic Horseshoe

The Cosmic Horseshoe (Belokurov et al. 2007) is an ideal test case for these methods. At  $z = 2.38$ , it is one of the best-studied gravitationally lensed galaxies. However, from the methods presented in Sect. 5, we would not expect the Cosmic Horseshoe to strongly emit ionizing photons. Restframe UV spectra from the MEGaSaURA sample (Fig. 5; Rigby et al. 2018) show a young stellar population with relatively deep Si II absorption lines (i.e., large  $C_f^{\text{Si}}$ ). Similarly, Ly $\alpha$  observations from the Echelle Spectrograph and Imager on the KECK II telescope only find  $f_{\text{esc}}^{\text{Ly}\alpha} = 0.08$  (Quider et al. 2009). Moreover, the Cosmic Horseshoe has a relatively small extinction-corrected  $O_{32}$  (2; Hainline et al. 2009). The suspicions of low  $f_{\text{esc}}$  are confirmed by deep HST LyC imaging that measures an upper limit of the absolute escape fraction of  $f_{\text{esc}}^{\text{obs}} < 0.02$  (Vasei et al. 2016). Vasei et al. (2016) noted that there was a 20% chance that the low  $f_{\text{esc}}^{\text{obs}}$  arises from IGM attenuation. While the IGM attenuation has a low-probability of impacting the  $f_{\text{esc}}^{\text{obs}}$ , proper simulations of the IGM opacity can quantify the impact of the IGM opacity at higher redshifts (Shapley et al. 2016).

From the stellar continuum fit in Fig. 5 (red line), we measured an  $E_{B-V}$  of 0.16 mag, consistent with Quider et al. (2009). The Si II 1260Å profile has a  $C_f^{\text{Si}}$  of 0.77 (corresponding to a H I covering fraction of  $C_f^{\text{pre, H}} = 0.94$  using Eq. 11). The escape fraction predicted using  $C_f^{\text{Si}}$  and Eq. 12 is  $f_{\text{esc}}^{\text{pre, Si}} = 0.009$ . The measured  $f_{\text{esc}}^{\text{Ly}\alpha} = 0.08$  leads to a LyC escape fraction of  $f_{\text{esc}}^{\text{pre, Ly}\alpha} = 0.012$  (Eq. 13). Finally, the extinction-corrected  $O_{32}$  is small, such that Eq. 15 implies a low  $f_{\text{esc}}^{\text{pre, O}} = 0.011$  (Eq. 15).

Combining the two robust estimates of  $f_{\text{esc}}^{\text{pre}}$  (the Si II and Ly $\alpha$  values), we derive a mean estimate of  $f_{\text{esc}}^{\text{pre}} = 0.011 \pm 0.002$  (Ta-

Table 3: Predicted Lyman continuum escape fractions for the 8 galaxies with predicted escape fractions higher than 0.01, but without Lyman series or Lyman continuum observations.

Galaxy Name	$z$	$E_{B-V}$ [mag]	$C_f^{\text{Si}}$	$f_{\text{esc}}^{\text{pre, Si}}$	$f_{\text{esc}}^{\text{pre, Ly}\alpha}$	$f_{\text{esc}}^{\text{pre}}$	$f_{\text{esc}}^{\text{obs}}$
(1)	(2)	(3)	(4)	(5)	(6)	(7)	(8)
<i>Ion2</i>	3.212	<0.04	-	-	>0.49	>0.49	$0.64_{-0.1}^{+1.1a}$
SDSS J1154+2443	0.3690	0.06	-	-	0.48	0.48	$0.46 \pm 0.02^b$
SGAS J211118.9–011431	2.8577	0.12	0.30	0.082	-	0.082	-
SGAS J142954.9–120239	2.8245	0.08	0.40	0.080	-	0.080	-
Haro 11	0.0206	0.12	0.60	0.036	-	0.036	$0.033 \pm 0.007^c$
SGAS J090003.3+223408	2.0326	0.11	0.65	0.026	0.025	$0.026 \pm 0.001$	$0.015 \pm 0.012^d$
SGAS J095738.7+050929	1.8204	0.21	0.63	0.013	-	0.013	-
SGAS J145836.1–002358	3.4868	0.07	0.83	0.011	-	0.011	-
The Cosmic Horseshoe	2.3812	0.16	0.77	0.009	0.012	$0.011 \pm 0.002$	$< 0.02^e$

**Notes.** Column 1 gives the galaxy name. Column 2 gives the redshifts of the galaxies. Column 3 and 4 give the stellar attenuation ( $E_{B-V}$ ) and Si II covering fraction ( $C_f^{\text{Si}}$ ) determined from a stellar continuum fit similar to the methods detailed in Sect. 2.2. Column 5 gives the Lyman continuum escape fraction predicted using the Si II 1260Å absorption line ( $f_{\text{esc}}^{\text{pre, Si}}$ ; Eq. 12). Column 6 gives the Lyman continuum escape fraction predicted by extinction correcting the Ly $\alpha$  escape fraction ( $f_{\text{esc}}^{\text{pre, Ly}\alpha}$ ; Eq. 14). Column 7 gives the mean and standard deviation of the predicted Lyman continuum escape fractions. Column 8 gives the observed Lyman continuum escape fraction ( $f_{\text{esc}}^{\text{obs}}$ ). The table is ordered in descending  $f_{\text{esc}}^{\text{pre}}$ . All of the galaxies, except *Ion2*, Haro 11, and J1154+2443 are drawn from the MEGaSAURA sample (Sect. 6.2; Rigby et al. 2018). Unmeasured quantities are denoted with dashes.

**References.** (a) de Barros et al. (2016); (b) Izotov et al. (2018); (c) Leitert et al. (2013); (d) This work (Sect. 6.2.1); (e) Vasei et al. (2016)

ble 4). This result is also consistent with the escape fraction predicted by the  $O_{32}$  scaling relation. The  $f_{\text{esc}}^{\text{pre}}$  satisfies the upper limit of the absolute escape  $f_{\text{esc}}^{\text{obs}} < 0.02$  from the HST imaging (Vasei et al. 2016).

## 6.2. Other MEGaSAURA galaxies

The Cosmic Horseshoe is one of 14 galaxies within the MEGaSAURA sample (three are included in the full sample in Table 2; Rigby et al. 2018). We also predicted the escape fraction for the full MEGaSAURA sample. Fitting the stellar continua and Si II 1260Å covering fractions of the sample predicts that only six (42%) have  $f_{\text{esc}}^{\text{pre, Si}} > 0.01$  (Table 3 gives the predicted escape fractions of these six galaxies). Two MEGaSAURA galaxies with low  $f_{\text{esc}}^{\text{pre, Si}} < 0.01$ , SGAS J1226+2152 and SGAS J1527+0652, also have low  $O_{32}$  values of 1.4 and 1.6, respectively (Table 2; Wuyts et al. 2012). These low  $O_{32}$  values correspond to  $f_{\text{esc}}^{\text{pre, O}} < 0.01$ , consistent with their low  $f_{\text{esc}}^{\text{pre, Si}}$ . No MEGaSAURA galaxy has  $f_{\text{esc}}^{\text{pre, Si}} > 0.1$ . This is consistent with the nondetection of LyC photons in the individual spectra (Rigby et al. 2018).

### 6.2.1. SGAS J0900+2234

SGAS J0900+2234, a  $z = 2.03$  lensed galaxy, is the second best MEGaSAURA test case. First, combining the rest-frame optical observations from Bian et al. (2010) with the MEGaSAURA data estimates the Ly $\alpha$  escape fraction to be 0.09 (Table 4). This  $f_{\text{esc}}^{\text{Ly}\alpha}$  leads to  $f_{\text{esc}}^{\text{pre, Ly}\alpha} = 0.025$ , consistent with the  $f_{\text{esc}}^{\text{pre, Si}} = 0.026$  (Table 3). There are no literature [O II] 3727Å observations for this galaxy. Consequently, we predicted  $f_{\text{esc}}^{\text{pre}} = 0.026 \pm 0.001$ .

This lensed galaxy has both LyC (F218W; rest-frame central wavelength of 734Å; PID: 13349; PI: X. Fan; Bian et al. 2017) and rest-frame FUV (F475W; rest-frame central wavelength of 1566Å; PID: 11602; PI: S. Allam) HST imaging. Bian

Table 4: Observed properties of SGAS J0900+2234

Row	Property	Value
(1)	$F[H\alpha]$	$(225 \pm 56) \times 10^{-17}$
(2)	$F[Ly\alpha]$	$(185 \pm 15) \times 10^{-17}$
(3)	$f_{\text{esc}}^{\text{Ly}\alpha}$	$0.09 \pm 0.02$
(4)	$F[1500]_{\text{obs}}$	$(6.9 \pm 0.4) \times 10^{-18}$
(5)	$F[900]_{\text{obs}}$	$(1.8 \pm 1.4) \times 10^{-19}$
(6)	$(F[1500]/F[900])_{\text{int}}$	1.4
(7)	$E_{B-V}$	$0.11 \pm 0.001$

**Notes.** Row 1 gives the extinction-corrected H $\alpha$  flux (Bian et al. 2010). Row 2 gives the observed Ly $\alpha$  flux. Row 3 gives the measured Ly $\alpha$  escape fraction. Row 4 gives the measured flux at 1500Å from the HST F475W image. Row 5 gives the measured flux at 912Å from the HST 218W image (Bian et al. 2017). Row 6 gives the ratio of the flux at 1500Å and 912Å from the stellar population fit. Row 7 gives the measured attenuation ( $E_{B-V}$ ; in mags) from the stellar population fit. All flux values have units of erg s $^{-1}$  cm $^{-2}$ .

et al. (2017) have not detected significant LyC photons from this lensed galaxy, but the HST images provide weak constraints on  $f_{\text{esc}}^{\text{obs}}$ . Following Eq. 1 from Leitert et al. (2013), we estimated  $f_{\text{esc}}^{\text{obs}}$  as

$$f_{\text{esc}}^{\text{obs}} = \frac{(F[1500]/F[900])_{\text{int}}}{(F[1500]/F[900])_{\text{obs}}} 10^{-0.4E_{B-V}k_{1500}} \quad (16)$$

where we took  $k_{1500}$  from the Reddy et al. (2016a) attenuation law and  $E_{B-V}$  from the STARBURST99 stellar continuum fit. The intrinsic flux ratio is measured from the STARBURST99 stellar population fit to the spectra (Table 4), and is similar to values from Izotov et al. (2016b) for an instantaneous 7 Myr stellar population (the fitted stellar age).  $(F[1500]/F[900])_{\text{obs}}$  is the observed ratio of the flux at 1500Å and 900Å, respectively. The  $F[1500]$  and  $F[900]$  values are measured from the exact same regions in the F475W and F218 images.  $F[900]$  has a low significance ( $1.3\sigma$ ; Table 4), which led Bian et al. (2017) to not report

a significant LyC detection. We measured  $f_{\text{esc}}^{\text{obs}} = 0.015 \pm 0.012$ , consistent, within  $1\sigma$ , with  $f_{\text{esc}}^{\text{pre}}$  (Table 3).

### 6.3. Haro 11

Haro 11, a nearby star-forming galaxy has a measured  $f_{\text{esc}}^{\text{obs}} = 0.033 \pm 0.007$  from Far-Ultraviolet Spectroscopic Explorer (FUSE) observations (Bergvall et al. 2006; Leitert et al. 2011). A recent HST/COS spectrum of Knot C in Haro 11 covers rest-frame 1130-1760Å (Heckman et al. 2011; Alexandroff et al. 2015). We measured  $E_{B-V} = 0.124$  mags and  $C_f^{\text{Si}} = 0.60$  from this COS spectrum (Chisholm et al. 2016). This  $C_f^{\text{Si}}$  value agrees with the recent value from Rivera-Thorsen et al. (2017) and leads to  $f_{\text{esc}}^{\text{pre, Si}} = 0.036$ . Keenan et al. (2017) have measured the O<sub>32</sub> of Haro 11 using HST/WFC3 imaging. While the imaging makes it challenging to robustly subtract the stellar continuum, the O<sub>32</sub> ratio is between 2–4 for Knot C. This corresponds to a  $f_{\text{esc}}^{\text{pre, O}} = 0.01 - 0.03$  (Eq. 15). Both  $f_{\text{esc}}^{\text{pre, Si}}$  and  $f_{\text{esc}}^{\text{pre, O}}$  are broadly consistent, within  $1\sigma$ , with  $f_{\text{esc}}^{\text{obs}}$ .

### 6.4. J1154+2443

Izotov et al. (2018) have recently discovered a new low-redshift LyC emitter, J1154+2443, with HST/COS spectra. At  $f_{\text{esc}}^{\text{obs}} = 0.46 \pm 0.02$ , it has the highest observed escape fraction in the local universe. Izotov et al. (2018) have listed properties of J1154+2443 that nicely align with those that we suggest lead to a high  $f_{\text{esc}}^{\text{obs}}$ : low metallicity ( $12 + \log(\text{O}/\text{H}) = 7.65$ ), low extinction ( $A_V = 0.145$ , or  $E_{B-V} = 0.06$  using their  $R_V = 2.4$ ), high  $f_{\text{esc}}^{\text{Ly}\alpha}$  ( $f_{\text{esc}}^{\text{Ly}\alpha} = 0.98$ ), and large O<sub>32</sub> (O<sub>32</sub> = 11.5). Using the  $f_{\text{esc}}^{\text{Ly}\alpha}$  and converting the attenuation measured with the Cardelli et al. (1989) curve to an attenuation using the Reddy et al. (2016a) relation, we predict that J1154+2443 would have  $f_{\text{esc}}^{\text{pre, Ly}\alpha} = 0.48$  (Table 3). This is consistent with  $f_{\text{esc}}^{\text{obs}}$  found by Izotov et al. (2018). In Sect. 5.3 we found the O<sub>32</sub> relation underpredicts the  $f_{\text{esc}}^{\text{pre, O}}$  of this galaxy by  $3\sigma$ . This suggests that more observations are required to better constrain the O<sub>32</sub> relation at large O<sub>32</sub>.

### 6.5. High-redshift LyC emitters

While most of the confirmed LyC detections have come at low redshift ( $z < 0.4$ ), four  $z \sim 3 - 4$  galaxies have confirmed  $f_{\text{esc}}^{\text{obs}}$  (Vanzella et al. 2015; de Barros et al. 2016; Shapley et al. 2016; Bian et al. 2017; Vanzella et al. 2018). These galaxies are typically more extreme LyC emitters than the  $z \sim 0$  galaxies ( $f_{\text{esc}}^{\text{obs}} = 0.2 - 0.7$ ) and have characteristics that Sect. 5 suggests lead to high  $f_{\text{esc}}^{\text{obs}}$ : low  $E_{B-V}$ , weak Si II absorption lines, and strong Ly $\alpha$ . *Ion2* (Vanzella et al. 2015) is the only high-redshift galaxy with literature limits for O<sub>32</sub> or  $f_{\text{esc}}^{\text{Ly}\alpha}$ , while no high-redshift galaxy has a published  $C_f^{\text{Si}}$ . *Ion2* has an extreme  $f_{\text{esc}}^{\text{obs}} = 0.64_{-0.1}^{+1.1}$ , an upper limit of O<sub>32</sub> > 15, a very low dust extinction upper limit ( $E_{B-V} < 0.04$  mag), a large lower limit of  $f_{\text{esc}}^{\text{Ly}\alpha} > 0.78$ , and a nondetected Si II 1260Å absorption line (de Barros et al. 2016). Using the methods in Sect. 5 we predict  $f_{\text{esc}}^{\text{pre, O}} > 0.39$  and  $f_{\text{esc}}^{\text{pre, Ly}\alpha} > 0.49$ . These predicted lower limits of the LyC escape fraction are consistent with  $f_{\text{esc}}^{\text{obs}} = 0.64$  from de Barros et al. (2016).

### 6.6. Prospects for the epoch of reionization

The above examples indicate that the methods from Sect. 5 can powerfully predict the  $f_{\text{esc}}$  of high-redshift galaxies. *JWST* and ELTs will observe the rest-frame UV of field and lensed  $z = 6 - 8$  galaxies to estimate  $f_{\text{esc}}^{\text{pre, Si}}$ . Additionally, optical emission lines will be redshifted to 3.5–4.5  $\mu\text{m}$ , such that the NIR-Spec instrument on *JWST* will measure H $\alpha$  and O<sub>32</sub>. These observations will estimate  $f_{\text{esc}}^{\text{pre, Ly}\alpha}$  and  $f_{\text{esc}}^{\text{pre, O}}$ . Combined, the three methods predict  $f_{\text{esc}}$  values that are broadly consistent with the observed escape fractions of local Lyman continuum emitting galaxies. The escape fractions, the total number of ionizing photons, and the luminosity functions will then describe whether star-forming galaxies reionized the  $z = 6 - 8$  universe.

## 7. Summary

We analyzed the rest-frame UV spectra of nine low-redshift ( $z < 0.3$ ) star-forming galaxies that emit ionizing photons. In a companion paper (Gazagnes et al. 2018), we fit the stellar continuum, dust attenuation, Lyman series absorption lines (H I absorption lines blueward of Ly $\alpha$ ), and ISM metal absorption lines. Here, we combined the H I column densities and covering fractions with the dust attenuations to predict the fraction of ionizing photons that escape local galaxies. The Lyman continuum and Lyman series both directly trace the escape of ionizing photon, but neither are observable at redshifts greater than 4. Therefore, we tested three indirect ways of estimating  $f_{\text{esc}}$ : the Si II absorption lines (Sect. 5.1), the Ly $\alpha$  escape fraction (Sect. 5.2), and the [O III]/[O II] flux ratio (Sect. 5.3). We then used these methods to predict the escape fractions of galaxies without Lyman series observations to illustrate how these indirect methods can estimate the escape fraction of high-redshift galaxies (Sect. 6).

The major results of this study are as follows:

1. The radiative transfer equation (Eq. 5), along with the fits to the dust attenuation, H I covering fraction, and H I column density reproduce the observed  $f_{\text{esc}}$  to within  $1.4\sigma$  (Fig. 1). The Lyman series absorption properties accurately predict the escape fraction of ionizing photons.
2. As shown in Gazagnes et al. (2018), the observed H I column densities indicate that the Lyman continuum is optically thick. Instead, ionizing photons escape because the covering fraction is less than one (Fig. 2).
3. The covering fraction alone overpredicts the escape fraction. While geometry dependent (see the discussion in Sect 3.1), dust attenuation is a key ingredient for the escape of ionizing photons (Fig. 2). Estimating the escape fraction as  $(1-C_f)$  will overestimate the true escape fraction.
4. Indirect methods also provide accurate estimates of the escape fraction of ionizing photons. The Si II absorption line and extinction-correction Ly $\alpha$  escape fraction predicts  $f_{\text{esc}}$  with similar accuracy as the Lyman series (Fig. 3), while the square of the [O III]/[O II] flux ratio scales strongly with  $f_{\text{esc}}$  ( $3\sigma$  significance; Fig. 4). The [O III]/[O II] relation agrees with previous studies for low [O III]/[O II] values, but underpredicts the  $f_{\text{esc}}$  of higher [O III]/[O II] values. This suggests that a larger sample of large [O III]/[O II] galaxies is required to constrain the full trend.
5. We applied the indirect methods to galaxies without Lyman series observations to illustrate how these methods predict  $f_{\text{esc}}$  (Table 3). In all cases, the  $f_{\text{esc}}$  values predicted with indirect methods are consistent with either the observed  $f_{\text{esc}}$  or upper limits of  $f_{\text{esc}}$ . Most (58%) of the  $z =$

1.7 – 3.6 MEGaSaURA galaxies have low escape fractions ( $f_{\text{esc}} \leq 1\%$ ), while the remaining galaxies have predicted  $f_{\text{esc}} \sim 1 - 8\%$  (Sect. 6.2). Additionally, the predicted escape fraction of J1154+2443, a recently discovered local galaxy with a high escape fraction (0.46), agrees with the observed value. Overall, the predicted  $f_{\text{esc}}$  values are consistent with the observed escape fractions.

This analysis presents new methods to measure and analyze the escape fractions of galaxies in the epoch of reionization using *JWST* and future ELT (Sect. 6.6). Deep rest-frame UV and optical spectroscopy of these high-redshift galaxies may determine whether high-redshift galaxies emit sufficient ionizing photons to reionize the universe or if other sources are required.

## References

- Ahn, C. P., Alexandroff, R., Allende Prieto, C., et al. 2014, *ApJS*, 211, 17
- Alexandroff, R. M., Heckman, T. M., Borthakur, S., Overzier, R., & Leitherer, C. 2015, *ApJ*, 810, 104
- Barlow, T. A. & Sargent, W. L. W. 1997, *AJ*, 113, 136
- Becker, R. H., Fan, X., White, R. L., et al. 2001, *AJ*, 122, 2850
- Belokurov, V., Evans, N. W., Moiseev, A., et al. 2007, *ApJ*, 671, L9
- Bergvall, N., Zackrisson, E., Andersson, B.-G., et al. 2006, *A&A*, 448, 513
- Bian, F., Fan, X., Bechtold, J., et al. 2010, *ApJ*, 725, 1877
- Bian, F., Fan, X., McGreer, I., Cai, Z., & Jiang, L. 2017, *ApJ*, 837, L12
- Bolton, J. S. & Haehnelt, M. G. 2007, *MNRAS*, 382, 325
- Borthakur, S., Heckman, T. M., Leitherer, C., & Overzier, R. A. 2014, *Science*, 346, 216
- Bouwens, R. J., Illingworth, G. D., Blakeslee, J. P., & Franx, M. 2006, *ApJ*, 653, 53
- Bouwens, R. J., Illingworth, G. D., Oesch, P. A., et al. 2012a, *ApJ*, 754, 83
- Bouwens, R. J., Illingworth, G. D., Oesch, P. A., et al. 2015, *ApJ*, 803, 34
- Bouwens, R. J., Illingworth, G. D., Oesch, P. A., et al. 2012b, *ApJ*, 752, L5
- Bruzual, G. & Charlot, S. 2003, *MNRAS*, 344, 1000
- Cardelli, J. A., Clayton, G. C., & Mathis, J. S. 1989, *ApJ*, 345, 245
- Chisholm, J., Orlitová, I., Schaerer, D., et al. 2017, *A&A*, 605, A67
- Chisholm, J., Tremonti, C. A., Leitherer, C., Chen, Y., & Wofford, A. 2016, *MNRAS*, 457, 3133
- de Barros, S., Vanzella, E., Amorín, R., et al. 2016, *A&A*, 585, A51
- Dijkstra, M., Gronke, M., & Venkatesan, A. 2016, *ApJ*, 828, 71
- Dressler, A., Henry, A., Martin, C. L., et al. 2015, *ApJ*, 806, 19
- Dunlop, J. S., McLure, R. J., Robertson, B. E., et al. 2012, *MNRAS*, 420, 901
- Faisst, A. L. 2016, *ApJ*, 829, 99
- Fan, X., Strauss, M. A., Becker, R. H., et al. 2006, *AJ*, 132, 117
- Finkelstein, S. L., Ryan, Jr., R. E., Papovich, C., et al. 2015, *ApJ*, 810, 71
- Fontanot, F., Cristiani, S., & Vanzella, E. 2012, *MNRAS*, 425, 1413
- Gazagnes, S., Chisholm, J., Schaerer, D., et al. 2018, *ArXiv:1802.06378*
- Green, J. C., Froning, C. S., Osterman, S., et al. 2012, *ApJ*, 744, 60
- Gunn, J. E. & Peterson, B. A. 1965, *ApJ*, 142, 1633
- Hainline, K. N., Shapley, A. E., Kornei, K. A., et al. 2009, *ApJ*, 701, 52
- Hamann, F., Barlow, T. A., Junkkarinen, V., & Burbidge, E. M. 1997, *ApJ*, 478, 80
- Harikane, Y., Ouchi, M., Shibuya, T., et al. 2017, *ArXiv e-prints*
- Heckman, T. M., Alexandroff, R. M., Borthakur, S., Overzier, R., & Leitherer, C. 2015, *ApJ*, 809, 147
- Heckman, T. M. & Borthakur, S. 2016, *ApJ*, 822, 9
- Heckman, T. M., Borthakur, S., Overzier, R., et al. 2011, *ApJ*, 730, 5
- Henry, A., Scarlata, C., Martin, C. L., & Erb, D. 2015, *ApJ*, 809, 19
- Hopkins, P. F., Hernquist, L., Cox, T. J., & Kereš, D. 2008, *ApJS*, 175, 356
- Ishigaki, M., Kawamata, R., Ouchi, M., Oguri, M., & Shimasaku, K. 2017, *ArXiv e-prints*
- Izotov, Y. I., Orlitová, I., Schaerer, D., et al. 2016a, *Nature*, 529, 178
- Izotov, Y. I., Schaerer, D., Thuan, T. X., et al. 2016b, *MNRAS*, 461, 3683
- Izotov, Y. I., Schaerer, D., Worseck, G., et al. 2018, *MNRAS*, 474, 4514
- Jaskot, A. E. & Oey, M. S. 2013, *ApJ*, 766, 91
- Jones, T., Stark, D. P., & Ellis, R. S. 2012, *ApJ*, 751, 51
- Jones, T. A., Ellis, R. S., Schenker, M. A., & Stark, D. P. 2013, *ApJ*, 779, 52
- Keenan, R. P., Oey, M. S., Jaskot, A. E., & James, B. L. 2017, *ApJ*, 848, 12
- Kuhlen, M. & Faucher-Giguère, C.-A. 2012, *MNRAS*, 423, 862
- Leethochawalit, N., Jones, T. A., Ellis, R. S., Stark, D. P., & Zitrin, A. 2016, *ApJ*, 831, 152
- Leitet, E., Bergvall, N., Hayes, M., Linné, S., & Zackrisson, E. 2013, *A&A*, 553, A106
- Leitet, E., Bergvall, N., Piskunov, N., & Andersson, B.-G. 2011, *A&A*, 532, A107
- Leitherer, C. & Heckman, T. M. 1995, *ApJS*, 96, 9
- Leitherer, C., Hernandez, S., Lee, J. C., & Oey, M. S. 2016, *ApJ*, 823, 64
- Leitherer, C., Ortiz Otálvaro, P. A., Bresolin, F., et al. 2010, *ApJS*, 189, 309
- Leitherer, C., Schaerer, D., Goldader, J. D., et al. 1999, *ApJS*, 123, 3
- Livermore, R. C., Finkelstein, S. L., & Lotz, J. M. 2017, *ApJ*, 835, 113
- Madau, P. & Dickinson, M. 2014, *ARA&A*, 52, 415
- Madau, P., Haardt, F., & Rees, M. J. 1999, *ApJ*, 514, 648
- Markwardt, C. B. 2009, in *Astronomical Society of the Pacific Conference Series*, Vol. 411, *Astronomical Data Analysis Software and Systems XVIII*, ed. D. A. Bohlender, D. Durand, & P. Dowler, 251
- Marshall, J. L., Burles, S., Thompson, I. B., et al. 2008, in *Proc. SPIE*, Vol. 7014, *Ground-based and Airborne Instrumentation for Astronomy II*, 701454
- Meiksin, A. 2005, *MNRAS*, 356, 596
- Meynet, G., Maeder, A., Schaller, G., Schaerer, D., & Charbonnel, C. 1994, *A&AS*, 103, 97
- Nagao, T., Maiolino, R., & Marconi, A. 2006, *A&A*, 459, 85
- Nakajima, K. & Ouchi, M. 2014, *MNRAS*, 442, 900
- Nakajima, K., Ouchi, M., Shimasaku, K., et al. 2013, *ApJ*, 769, 3
- Oesch, P. A., Bouwens, R. J., Illingworth, G. D., et al. 2014, *ApJ*, 786, 108
- Oesch, P. A., Bouwens, R. J., Illingworth, G. D., Labbe, I., & Stefanon, M. 2017, *ArXiv e-prints*
- Onoue, M., Kashikawa, N., Willott, C. J., et al. 2017, *ApJ*, 847, L15
- Ouchi, M., Ono, Y., Egami, E., et al. 2009, *ApJ*, 696, 1164
- Planck Collaboration, Adam, R., Aghanim, N., et al. 2016, *A&A*, 596, A108
- Puschnig, J., Hayes, M., Östlin, G., et al. 2017, *ArXiv e-prints*
- Quider, A. M., Pettini, M., Shapley, A. E., & Steidel, C. C. 2009, *MNRAS*, 398, 1263
- Reddy, N. A., Steidel, C. C., Pettini, M., & Bogosavljević, M. 2016a, *ApJ*, 828, 107
- Reddy, N. A., Steidel, C. C., Pettini, M., Bogosavljević, M., & Shapley, A. E. 2016b, *ApJ*, 828, 108
- Ricci, F., Marchesi, S., Shankar, F., La Franca, F., & Civano, F. 2017, *MNRAS*, 465, 1915
- Rigby, J. R., Bayliss, M. B., Sharon, K., et al. 2018, *AJ*, 155, 104
- Rivera-Thorsen, T. E., Östlin, G., Hayes, M., & Puschnig, J. 2017, *ApJ*, 837, 29
- Robertson, B. E., Ellis, R. S., Furlanetto, S. R., & Dunlop, J. S. 2015, *ApJ*, 802, L19
- Robertson, B. E., Furlanetto, S. R., Schneider, E., et al. 2013, *ApJ*, 768, 71
- Sanders, R. L., Shapley, A. E., Kriek, M., et al. 2016, *ApJ*, 816, 23
- Schaerer, D. & de Barros, S. 2010, *A&A*, 515, A73
- Schlegel, D. J., Finkbeiner, D. P., & Davis, M. 1998, *ApJ*, 500, 525
- Shapley, A. E., Reddy, N. A., Kriek, M., et al. 2015, *ApJ*, 801, 88
- Shapley, A. E., Steidel, C. C., Strom, A. L., et al. 2016, *ApJ*, 826, L24
- Songaila, A. 2004, *AJ*, 127, 2598
- Strom, A. L., Steidel, C. C., Rudie, G. C., Trainor, R. F., & Pettini, M. 2017, *ArXiv e-prints*
- Vanzella, E., de Barros, S., Castellano, M., et al. 2015, *A&A*, 576, A116
- Vanzella, E., de Barros, S., Vasei, K., et al. 2016, *ApJ*, 825, 41
- Vanzella, E., Grazian, A., Hayes, M., et al. 2010, *A&A*, 513, A20
- Vanzella, E., Nonino, M., Cupani, G., et al. 2018, *MNRAS*
- Vasei, K., Siana, B., Shapley, A. E., et al. 2016, *ApJ*, 831, 38
- Verhamme, A., Orlitová, I., Schaerer, D., & Hayes, M. 2015, *A&A*, 578, A7
- Verhamme, A., Orlitová, I., Schaerer, D., et al. 2017, *A&A*, 597, A13
- Wakker, B. P., Hernandez, A. K., French, D. M., et al. 2015, *ApJ*, 814, 40
- Willott, C. J., Delorme, P., Reyly, C., et al. 2010, *AJ*, 139, 906
- Worseck, G., Prochaska, J. X., Hennawi, J. F., & McQuinn, M. 2016, *ApJ*, 825, 144
- Worseck, G., Prochaska, J. X., O'Meara, J. M., et al. 2014, *MNRAS*, 445, 1745
- Wuyts, E., Rigby, J. R., Gladders, M. D., et al. 2012, *ApJ*, 745, 86
- Zackrisson, E., Inoue, A. K., & Jensen, H. 2013, *ApJ*, 777, 39